J. Phys.: Condens. Matter **10** (1998) 7879–7896. Printed in the UK PII: S0953-8984(98)94187-X

Electron spin resonance in the doped spin–Peierls compound $Cu_{1-x}Ni_xGeO_3$

V N Glazkov†, A I Smirnov†, O A Petrenko‡, D M^{c}K Paul‡, A G Vetkin§ and R M Eremina‖

† P L Kapitza Institute for Physical Problems RAS, 117334 Moscow, Russia
‡ Department of Physics, University of Warwick, Coventry CV4 7AL, UK
§ M V Lomonosov Moscow State University, 119899 Moscow, Russia
‖ E K Zavoisky Physical Technical Institute, 420029 Kazan, Russia

Received 8 May 1998

Abstract. Electron spin-resonance studies of the Ni-doped spin–Peierls compound $CuGeO_3$ have been performed for the frequency range 9–75 GHz and temperature interval 1.3–20 K. An anomalous temperature dependence of the g-factor below the spin–Peierls temperature was observed for doped samples. At low temperatures the g-factor is much smaller than the value expected for Cu^{2+} and Ni^{2+} ions and is much more anisotropic than for an undoped crystal. This anomaly is explained by the formation of magnetic clusters around the Ni^{2+} ions within a nonmagnetic spin–Peierls matrix. The formation of magnetic clusters is confirmed by the observation of a nonlinear static magnetic susceptibility at low temperatures.

The reduction of the spin–Peierls transition temperature was found to be linear in the dopant concentration x over the range $0 \leqslant x \leqslant 3.2\%$. The transition into the antiferromagnetically ordered state, detected earlier by neutron scattering for $x \geqslant 1.7\%$, was studied by means of ESR. For $x = 3.2\%$ a gap in the magnetic resonance spectrum is found below the Néel temperature and the spectrum is well described by the theory of antiferromagnetic resonance based on the molecular-field approximation. For $x = 1.7\%$ the spectrum below the Néel point remained gapless. The gapless spectrum of the antiferromagnetic state in weakly doped samples is attributed to the small value of the Néel order parameter and to the magnetically disordered spin–Peierls background.

1. Introduction

The magnetic properties of crystals of the quasi-one-dimensional magnet $CuGeO_3$ have been extensively studied since Hase *et al* [1] reported that this compound is the first inorganic spin–Peierls material. The spin–Peierls transition occurs because the $S = 1/2$ Heisenberg antiferromagnetic chains are unstable when coupled to a three-dimensional phonon field [2]. Below the transition temperature the magnetic chains are dimerized and the distance between the neighbouring magnetic ions as well as the exchange integral alternate. The positions of pairs of magnetic ions after the dimerization are correlated between neighbouring chains. Thus the dimers construct an ordered sublattice.

The dimerization of the magnetic ions in chains arranged along the c-direction of the orthorhombic crystal leads to the formation of the nonmagnetic ground state separated from the excited triplet states by an energy gap $\Delta \approx 2$ meV ≈ 23 K [3]. The unit cell in the dimerized state is doubled along the a- and c-directions and the intrachain exchange integral takes the alternating values $J_{1,2} = (1 \pm \delta)J_c$. Here $J_c = 10.2$ meV is the intrachain exchange

0953-8984/98/357879+18$19.50

integral and $\delta \approx 0.04$ is a distortion parameter [4]. The existence of such dimerization was confirmed by the observation of additional reflections by x-ray [5] and neutron [4] diffraction. Since the thermally excited triplet states are separated from a nonmagnetic ground state by an energy gap, the number of excitations and the magnetic susceptibility should decrease and tend to zero below the transition temperature. Both static susceptibility measurements [1] and ESR studies [6–8] performed on crystals of pure $CuGeO_3$ showed that the susceptibility rapidly decreases below $T_{SP} = 14.5$ K. The temperature of the transition to the dimerized state was obtained from the initial decrease in susceptibility.

$CuGeO_3$ is not a perfect one-dimensional magnet; the intrachain exchange J_c is larger but not much stronger than the interchain exchanges $J_b = 0.1J_c$ and $J_a = -0.01J_c$ [3]. A next-nearest-neighbour exchange along the chains with a significant value of $J' \approx 0.36J_c$ also probably exists in this compound [9–11]. If the crystal lattice of $CuGeO_3$ was harder, this crystal would be antiferromagnetic due to the intra- and interchain exchange interactions with a Néel temperature of about [12]

$$T_N \sim (J_c J_b)^{1/2} \sim 10 \text{ K}.$$

But the spin–Peierls state wins the competition with long-range antiferromagnetic order. Doping by impurities makes long-range antiferromagnetic order possible again. The presence of impurities diminishes the temperature of the spin–Peierls transition and at lower temperatures a Néel ordering occurs [13, 14]. The spin–Peierls dimerization and the antiferromagnetism were found to coexist in doped crystals. This phenomenon was explained by Fukuyama *et al* [15] and Khomskii *et al* [11], who showed by different methods that the impurity or the defect in the dimerization should be surrounded by a region of antiferromagnetically correlated spins, forming magnetic clusters, or solitons. The tails of these solitons could overlap, producing long-range magnetic order. From such a point of view, the reduction of the spin–Peierls temperature is proportional to the concentration of the dopant for small concentrations.

The impurity or the point magnetic defect inserted into the nonmagnetic spin–Peierls matrix generates a 'many-spin' object consisting of the impurity itself and of several neighbouring Cu-ion spins. The magnetic object formed due to the presence of the impurity is therefore a mesoscopic-type object containing a number of spins which is intermediate between microscopic and macroscopic systems, while the magnetization remains microscopic.

Single crystals of $CuGeO_3$ with the following substituting impurities were investigated: Si, Ti on the Ge sites [13, 16], Zn, Mg [17–19], Ni [20, 21] and Co [22] on the Cu sites. The suppression of the spin–Peierls transition and occurrence of antiferromagnetic order at low temperatures are common features for different dopants. In the antiferromagnetic phase the magnetic moment per Cu ion is strongly reduced. This reduction depends upon the type of dopant and their concentration. For the 3.2% Ni-doped crystal the effective moment is $\mu_{eff} = (0.16 \pm 0.03)\mu_B$ while it decreases to $(0.06 \pm 0.03)\mu_B$ for the 1.7% Ni-doped sample [20]. For the 3.2% Zn-doped crystal $\mu_{eff} \approx 0.2\mu_B$ [23]. The direction of the easy axis of the antiferromagnetically ordered state also depends on the dopant: the easy axis is directed along the *c*-axis for Zn [8], Si [24], Co [22], while for the Ni-doped crystals it is directed along the *a*-axis [21].

The aim of the present paper was the study of the ESR signals from the impurity-seeded magnetic clusters and the search for the antiferromagnetic resonance (AFMR) in the Ni-doped single crystals $Cu_{1-x}Ni_xGeO_3$. These were the same crystals as were investigated earlier by means of neutron scattering [20].

2. Experimental details and samples

In our experiments we used a set of ESR spectrometers with transmission-type cavities in the frequency range 8–80 GHz. The microwave cavities were placed in a hermetically isolated volume immersed in a liquid helium bath and filled with a small amount of He gas, enabling one to vary the temperature of the cavity containing the sample over the range 1.3–20 K. The magnetic resonance absorption lines were recorded through the dependence of the transmitted microwave power on the applied magnetic field. The reduction of the transmitted power is proportional to the power absorbed by the sample when the absorbed power is low. In the paramagnetic state the intensity of the absorption integrated over the magnetic field is proportional to the static susceptibility of the spin system.

The magnetization curves were obtained using an Oxford Instruments vibrating-sample magnetometer.

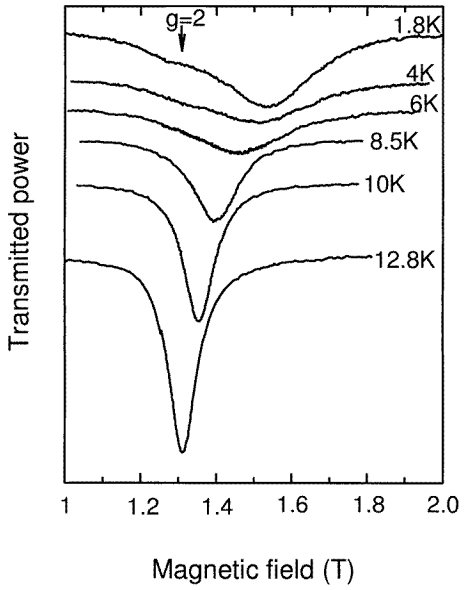

Figure 1. The temperature evolution of the ESR line for the 0.5% Ni-doped sample. $\boldsymbol{H} \parallel \boldsymbol{c}$, $f = 36.7$ GHz. The arrow marks the resonance field of the free-electron spin ($g = 2$).

Single crystals of $Cu_{1-x}Ni_xGeO_3$ with $x = 0.017$ and $x = 0.032$ were produced by the crystal growth procedure described in [20]. These were the same samples as had been used for neutron scattering experiments. These experiments showed the appearance of antiferromagnetic order at $T_N = 2.3$ K in the 1.7% Ni-doped crystal and at 4.2 K for $x = 3.2\%$. The transition to the spin–Peierls state at $T_{SP} = 11.5$ K was observed for the 1.7% Ni-doped crystal, while for the sample containing 3.2% Ni the spin–Peierls transition was not clearly observed. The values of the exchange integrals $J_b = 0.7 \pm 0.1$ meV, $J_c = 1.8 \pm 0.3$ meV and of the spin-wave energy gap $\Delta \approx 0.18$ meV were obtained from the dispersion curves of the magnetic excitations in the 3.2% Ni-doped $CuGeO_3$ at $T = 1.5$ K. To investigate the influence of the Ni doping at low concentrations, when the dopant atoms do not interact, crystals of $Cu_{1-x}Ni_xGeO_3$ with $x \leqslant 0.005$ were grown by recrystallization of ceramic samples in air using a horizontal floating-zone method. The growth rate was 5–7 mm h^{-1}. The ceramic samples were prepared by the

annealing in air of a nonstoichiometric mixture of CuO, GeO_2 and Ni_2O_3 at 950 °C for 24 hours.

3. Experimental results

3.1. The temperature evolution of the ESR line and the AFMR spectrum

The evolution of the ESR line with temperature for the pure crystals of $CuGeO_3$ is described in [6–8]. The intensity of the resonance absorption diminishes rapidly below T_{SP}. The nonmonotonic change of the g-factors g_a, g_b and g_c takes place with the temperature variation in the range between 14.5 and 4 K. This change occurs near the values which are close to $g = 2.1$ and the magnitude of this change does not exceed 4% for g_a and g_b and 1% for g_c. The additional line with $g_a = 1.82$, $g_c = 1.45$, $g_b = 1.86$ occurs below 4 K. The main line splits into three narrow lines at low temperatures. At a temperature of 4 K the ESR integral intensity of pure samples from our set of crystals is about 3×10^{-3} of the intensity of a paramagnet with one electron spin per Cu ion. The residual ESR signal of the pure crystals is attributed to defects in the structure and to residual impurity content, as well as to the boundaries of the spin–Peierls domains [25].

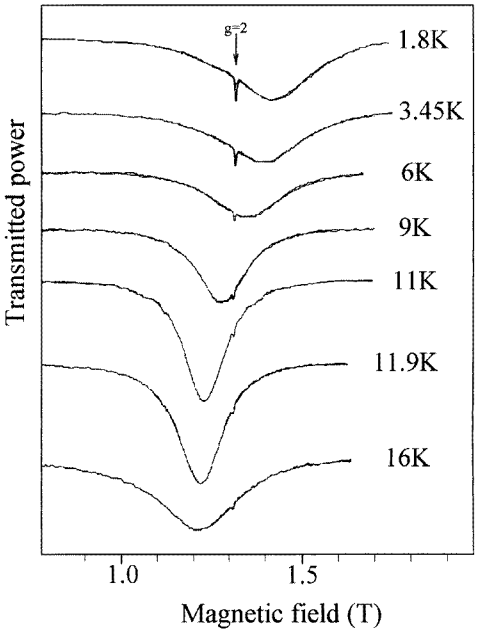

Figure 2. The temperature evolution of the ESR line for the 1.7% Ni-doped sample. $\boldsymbol{H} \parallel \boldsymbol{b}$, $f = 36.0$ GHz. The arrow marks the resonance field for $g = 2$. The narrow line is the DPPH mark.

The intensity of the ESR signals observed at low temperatures in the Ni-doped samples is larger than the intensity of the ESR in pure samples. The value of the intensity for $x = 0.5\%$ corresponds approximately to the concentration of the inserted impurities, while for $x \geqslant 1.7\%$ the intensity is less than that of a paramagnet with the corresponding amount of $S = 1$ spins. The evolution of the ESR line with temperature for samples with different concentrations of impurity is shown in figures 1, 2 and 3.

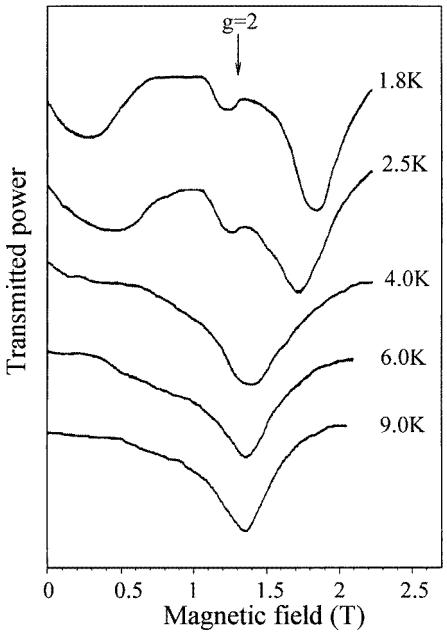

Figure 3. The temperature evolution of the ESR line for the 3.2% Ni-doped sample. $\boldsymbol{H} \parallel \boldsymbol{a}$ (easy-axis direction). The arrow marks the resonance field for $g = 2$.

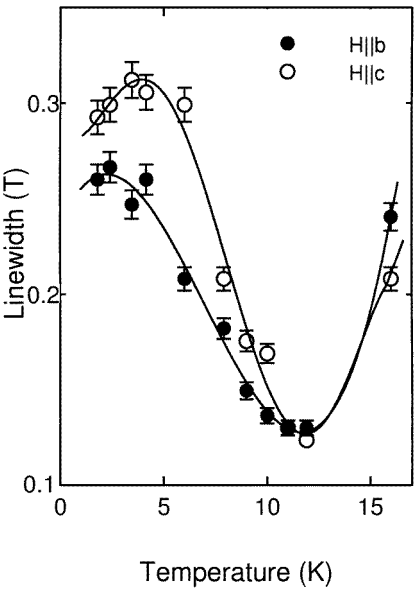

Figure 4. The temperature dependence of the ESR linewidth for the 1.7% Ni-doped sample. $f = 36.4$ GHz.

In contrast to the case for the pure material, the value of the g-factor strongly depends on the temperature below T_{SP} for Ni-doped crystals. The resonance field is shifted toward

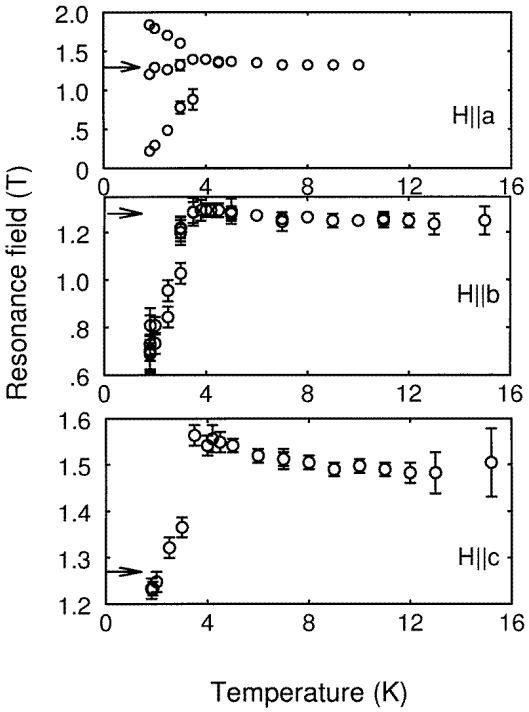

Figure 5. The temperature dependencies of resonance fields for the 3.2% Ni-doped sample. $f \approx 36$ GHz. The arrows mark the resonance fields for $g = 2$.

higher fields with decreasing temperature and the g-factor diminishes by about 20%. For the smallest concentration, $x = 0.005$ (figure 1), an additional weak line with a g-factor of about 2 arises at low temperatures, indicating an ESR spectrum which is intermediate between those of the pure and doped samples.

The sample doped with 1.7% Ni showed an analogous temperature shift of the ESR line (figure 2). The linewidth has a maximum at a temperature of about 2.5 K (see figure 4), which is close to the Néel temperature for this crystal. There is no observable shift of the line position between the Néel temperature 2.3 K and the lowest temperature of our experiments, 1.3 K, in the frequency range 18–60 GHz.

The sample containing 3.2% Ni demonstrated a transformation from a single-line spectrum into a spectrum typical of an orthorhombic antiferromagnet with several resonant lines. Three lines appear at this transformation when the magnetic field is parallel to the direction of spin ordering (figure 3), and a gap opens in the absorption spectrum for other directions of the magnetic field. This transformation occurs at 4 K, corresponding to the Néel temperature for this sample. Above the Néel temperature, the resonance field slightly increases as the temperature decreases, but this shift is smaller than for more lightly doped samples. The temperature evolution of the resonance field is given in figure 5.

We performed measurements of the resonance field in the frequency range 18–75 GHz. The resonance frequency–field dependencies for 0.5% Ni-doped and 1.7% Ni-doped samples were linear and gapless in the temperature interval between 1.3 and 20 K. A typical dependence of the resonance frequency f on the magnetic field H is given in figure 6. The temperature dependencies of the g-factors taken at different frequencies are given in

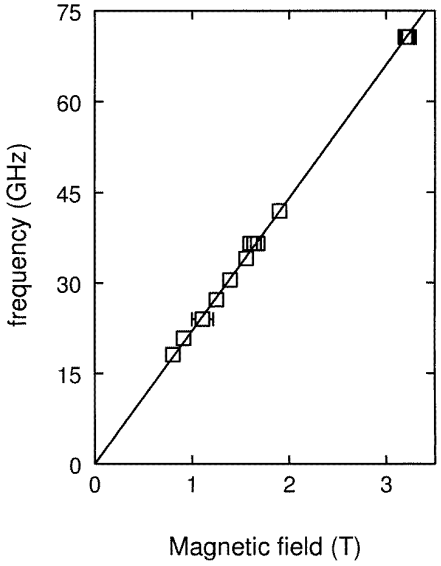

Figure 6. The ESR spectrum of the crystal doped with 1.7% Ni. $\boldsymbol{H} \parallel \boldsymbol{c}$, $T = 1.8$ K.

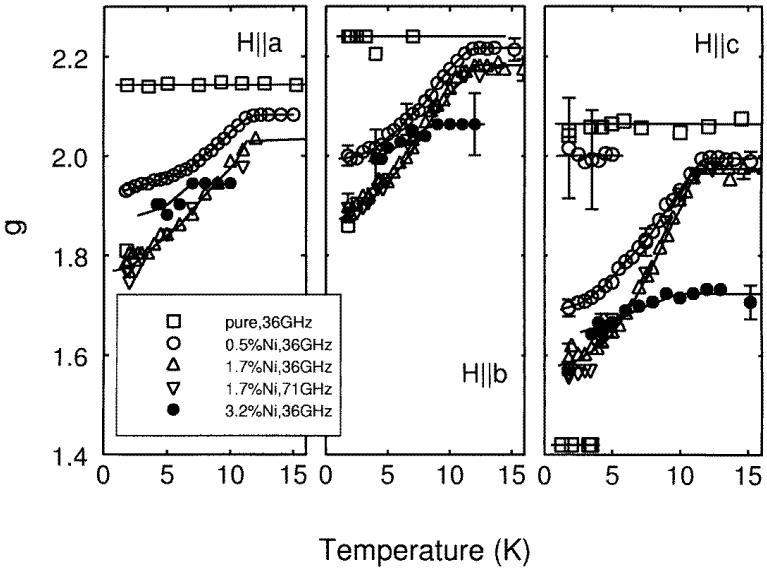

Figure 7. The temperature dependencies of the g-factors.

figure 7. The sample doped with 3.2% Ni is presented here only at $T \geqslant T_N$, where the spectrum is gapless. The values of the g-factors are obtained from the relation $g = 2f/\gamma H$ with $\gamma = 28$ GHz T^{-1}.

Note that the deviation of the g-factors with temperature does not tend towards the value of the g-factor for Ni^{2+} ions which has the value of about 2.3. At $T > T_{SP}$ there is also a remarkable deviation of the g-factor for the doped crystals from the value of the pure material. This deviation increases with increasing concentration.

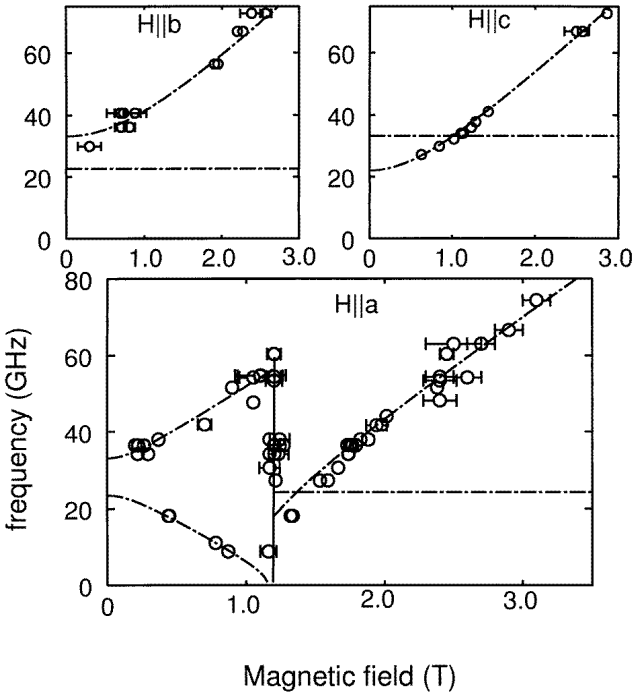

Figure 8. The spectrum of the antiferromagnetic resonance of $Cu_{0.968}Ni_{0.032}GeO_3$ at $T = 1.8$ K.

The AFMR spectrum of the 3.2% Ni-doped sample at $T = 1.8$ K which has well pronounced gaps of 22 GHz and 33 GHz is presented in figure 8.

3.2. The spin–Peierls transition

The drop of the integrated intensity of the ESR line marks the temperature of the spin–Peierls transition both for pure and doped crystals. The appropriate temperature dependence of the integrated intensity is shown in figures 9(a) and 9(b). The transition temperatures obtained from the ESR data are given in table 1.

Table 1. The temperatures of the spin–Peierls transition obtained from the ESR intensity versus temperature dependencies for the samples of $Cu_{1-x}Ni_xGeO_3$

x	0	0.5%	1.7%	3.2%
T_{SP} (K)	14.0 ± 0.5	12.5 ± 0.5	11.5 ± 0.5	8.0 ± 1

The values of T_{SP} for doped crystals are smaller than those for pure $CuGeO_3$. The value of T_{SP} for the 1.7% Ni-doped sample agrees well with the neutron scattering data [20], while for the 3.2% Ni-doped sample the neutron scattering data cannot be used for the determination of T_{SP} because of the almost complete collapse of the spin–Peierls excitations.

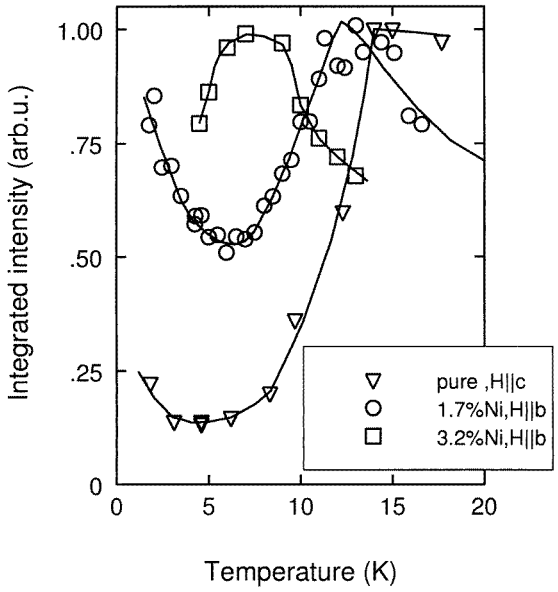

(a)

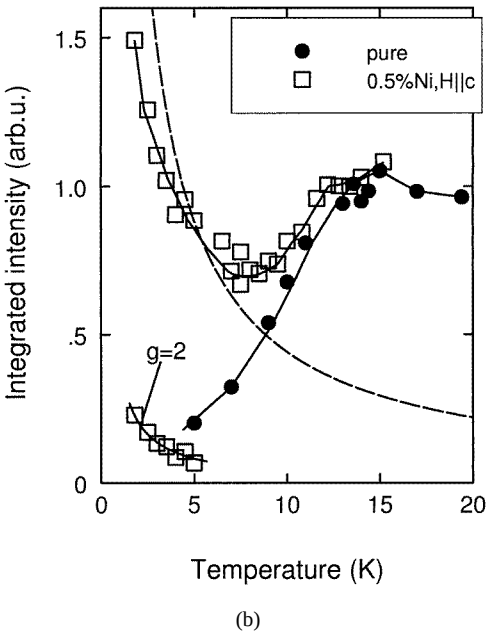

(b)

Figure 9. The temperature dependencies of the integrated ESR intensity for pure and doped crystals. The dotted curve shows the susceptibility of a paramagnet containing 0.5% of spins $S = 1$. $g = 2.3$.

3.3. Magnetization curves

The magnetization versus magnetic field was measured at different temperatures for the 1.7% Ni-doped sample to investigate the magnetic properties of the sample in the temperature

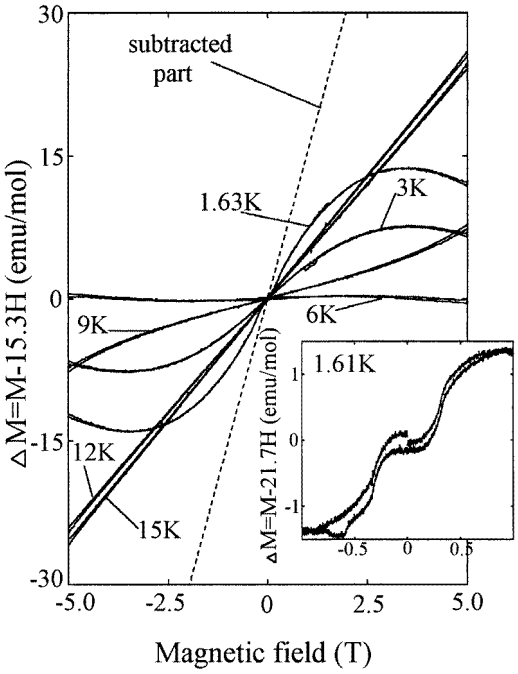

Figure 10. Magnetization curves for the 1.7% Ni-doped sample at $\boldsymbol{H} \parallel \boldsymbol{a}$.

range of the strong g-factor evolution. Figure 10 illustrates the $M(H)$ dependencies at different temperatures for $\boldsymbol{H} \parallel \boldsymbol{a}$. For the clear demonstration of the nonlinear contribution a fixed linear part is subtracted and the difference ΔM is plotted. Significant nonlinearity arises at low ($T < 6$ K) temperatures. The inset of this figure demonstrates the spin-flop transition at $H = 0.3$ T, $\boldsymbol{H} \parallel \boldsymbol{a}$. For $\boldsymbol{H} \parallel \boldsymbol{b}$ and $\boldsymbol{H} \parallel \boldsymbol{c}$ the $M(H)$ curves are similar except for the spin-flop steps, which are observable only for $\boldsymbol{H} \parallel \boldsymbol{a}$. The nonlinear parts for the a- and c-directions of the magnetic field are the same, for the b-direction the nonlinear contribution is about 50% greater.

4. Discussion

4.1. The x–T phase diagram

The values of the spin–Peierls transition temperature and the Néel points obtained from the ESR intensity are in good agreement with the x–T phase diagram for the Ni-doped samples presented in [26], with a linear decrease of T_{SP} with x in the interval 1.7–2.9%. Our additional points at $x = 0.5\%$ and 3.2% extend the experimental verification of the linear region.

4.2. Antiferromagnetic resonance

Doped crystals, which demonstrated the Néel order at low temperatures, show different types of magnetic resonance spectrum. The sample doped with 1.7% Ni has the Néel point at 2.3 K, but did not show a characteristic gap in the magnetic resonance spectrum (figure 6).

The sample doped with 3.2% Ni has a gap in the resonance spectrum (figure 8). This spectrum may be described as the AFMR spectrum of an orthorhombic antiferromagnet, obtained by means of the Landau–Lifshitz equations of sublattice magnetization motion within a molecular-field approximation. Taking the axes a, c, b as the easy, the second easy and the hard axis correspondingly, we obtain the resonance frequencies $\nu_{1,2}$ as follows [27].

(i) $\boldsymbol{H} \parallel \boldsymbol{a}$, $H < H_{SF}$:

$$(\nu_{1,2}/\gamma)^2 = \frac{1}{2}[(1+\alpha^2)H^2 + C_1 + C_2 \pm ((1-\alpha^2)^2H^4 + 2(1+\alpha)^2(C_1+C_2)H^2 + (C_1-C_2)^2)^{1/2}]. \tag{1}$$

(ii) $\boldsymbol{H} \parallel \boldsymbol{a}$, $H > H_{SF}$:

$$\begin{aligned}(\nu_1/\gamma)^2 &= H^2 - C_1\\ (\nu_2/\gamma)^2 &= C_2 - C_1.\end{aligned} \tag{2}$$

(iii) $\boldsymbol{H} \parallel \boldsymbol{c}$:

$$\begin{aligned}(\nu_1/\gamma)^2 &= H^2 + C_1\\ (\nu_2/\gamma)^2 &= C_2.\end{aligned} \tag{3}$$

(iv) $\boldsymbol{H} \parallel \boldsymbol{b}$:

$$\begin{aligned}(\nu_1/\gamma)^2 &= H^2 + C_2\\ (\nu_2/\gamma)^2 &= C_1.\end{aligned} \tag{4}$$

Here $C_{1,2} = 2H_eH_{a1,a2}$ (H_e, $H_{a1,a2}$ are exchange and anisotropy fields respectively), $H_{SF} = (2H_eH_{a1}/\alpha)^{1/2}$ is the spin-flop field and $\alpha = 1 - \chi_\parallel/\chi_\perp$. The applied magnetic field H and the anisotropy fields are considered to be much smaller than the exchange field.

By fitting our data according to equations (1)–(4) we obtained the following parameters of the AFMR spectrum:

$$\begin{aligned}H_{SF} &= 1.2 \pm 0.05 \text{ T}\\ \gamma &= 24.6 \text{ GHz T}^{-1}\\ 2H_eH_{a1} &= 0.85 \pm 0.10 \text{ T}^2\\ 2H_eH_{a2} &= 1.80 \text{ T}^2\\ \alpha &= 0.75 \pm 0.2.\end{aligned}$$

The gap values for the second easy- and hard-axis directions of the magnetic field are 22 GHz and 33 GHz (0.11 meV and 0.17 meV) respectively, which are in agreement with the value of 0.18 meV obtained from neutron scattering [20].

The spin-flop magnetic field is characterized by a wide band of absorption instead of a single resonance frequency (see figure 8). According to our data, $H_{SF} = 1.2$ T. This value is in good agreement with the value of the spin-flop field of 1.1 T found in [21] from magnetization curves for the Ni-doped crystal with $x = 0.033$.

From the exchange integral values $J_b \approx 0.7$ meV, $J_c \approx 1.8$ meV described in section 2 and assuming that $S = 1/2$ and $H_e = 4(J_c + J_b)S/(g\mu_B)$, we estimate the exchange-field value $H_e \approx 27$ T. Furthermore, from our data on the AFMR gap we deduce the values of the anisotropy fields: $H_{a1} \approx 0.017$ T and $H_{a2} \approx 0.036$ T.

The single-line ESR spectrum transforms into the AFMR spectrum with a gap for $x = 3.2\%$, but for $x = 1.7\%$ the transition to the Néel state is marked only by the maximum of the linewidth. If the conventional approach to the AFMR frequency derivation were valid

for the sample containing 1.7% Ni, the observed value of the spin-flop transition (figure 10) would correspond to an AFMR gap of 7.5 GHz. For the frequency 18 GHz, for $\boldsymbol{H} \parallel \boldsymbol{a}$ it should shift the resonance field by 0.05 T towards higher fields and for $\boldsymbol{H} \parallel \boldsymbol{c}$ to lower fields. This shift should be visible in our experiments on lowering the temperature from $T_N = 2.3$ to 1.3 K. Nevertheless, no shift exceeding 0.02 T was observed. This discrepancy between the static and dynamic properties of the impurity-induced antiferromagnetic state within the spin–Peierls matrix may be attributed to the low value of the order parameter for the Néel state. The sublattice magnetization equals only 0.06 of the nominal value. The usual procedure for deriving the AFMR frequency is therefore not valid, because of the assumption that the spins are arranged in the form of hard sublattices, without a reservoir of disordered spins. In the case of the coexistence of the spin–Peierls and Néel ordered states, the magnetically ordered part of the magnetization should interact with the disordered spin–Peierls background via the strong exchange interaction J_c. It will probably cause an unusual type of magnetic resonance frequency or an overdamped mode.

4.3. Spin clusters and magnetic resonance

The value of the g-factor for Ni-doped samples differs strongly from the corresponding values for pure crystals and for crystals doped with other impurities [24, 19]. This difference is found both above and below T_{SP}. Below the spin–Peierls transition there is also a strong anisotropy in the g-factor. Because of the pronounced difference between the observed g-factor and that expected for individual Ni and Cu ions, we consider that clusters of several spins coupled by the exchange interaction are responsible for the discrepancy. The g-factor of the cluster of ions coupled by the symmetric Heisenberg exchange takes the averaged value between the g-factors of isolated ions [28]. The observed g-factor value is well outside of this interval. The possible reason for this striking g-factor deviation is the formation of clusters containing several spins coupled both by symmetric and antisymmetric exchange interactions [29].

The formation of clusters should occur in doped $CuGeO_3$ crystals around the dopant ions, as described in section 1, because the defect is surrounded by several antiferromagnetically correlated spins. The characteristic length of the reduction of the correlated spin component on moving away from the impurity should be about seven interionic distances [11].

Clusters containing three $S = 1/2$ ions are known to display an effective g-factor which is smaller than the g-factor of an isolated ion. The anisotropy of the g-factor for the cluster is larger than that of the isolated ions [30, 31, 29]. This change in the g-factor is described by taking into account the spin–orbital interaction combined with the Heisenberg exchange in the form of a Dzyaloshinsky–Moriya antisymmetric exchange which is allowed when the symmetry of the pairs of the interacting ions is low enough. According to [29], the reduction of the effective g-factor is of the order of $D/\delta J$. Here D is the antisymmetric exchange coefficient and δJ is the difference between the exchange integrals within a triangular spin cluster. The presence of the Dzyaloshinsky–Moriya term for pure $CuGeO_3$ was proposed in [32] to explain the ESR linewidth at high temperatures. In addition, the Dzyaloshinsky–Moriya term describing the interaction of two neighbouring magnetic ions may arise below T_{SP} because of the lowering of the local symmetry resulting from the dimerization.

Figure 11 shows an impurity atom embedded in the dimerized matrix. The dimerization is disturbed in the vicinity of the impurity. There are no symmetry centres for Ni–Cu pairs. The region around the impurity atom also does not have a symmetry centre. Therefore Dzyaloshinsky–Moriya interaction coefficients should have different nonzero values for each pair of ions in the vicinity of the impurity.

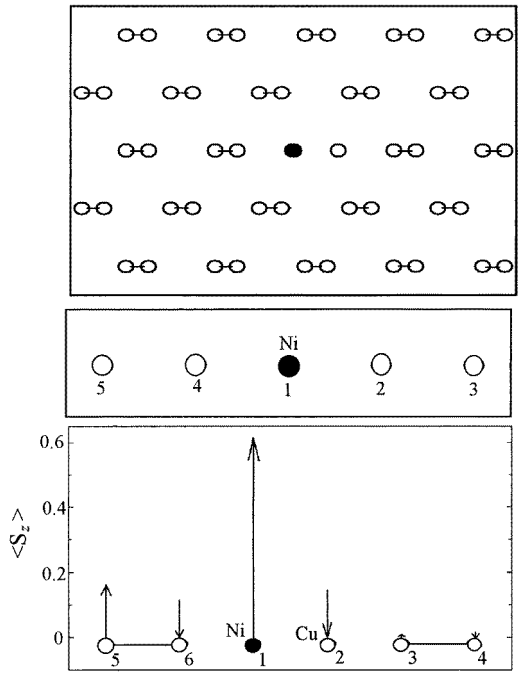

Figure 11. The structure of the dimerized lattice around the impurity atom. The five- and six-spin clusters. The arrows indicate the direction and the value of the average spin projections within the six-spin cluster with $D_{ij} = 0$.

We consider the models of the spin cluster with the final and relatively small numbers of spins to describe qualitatively the ESR spectra and to evaluate the coefficients of the Dzyaloshinsky–Moriya interaction. The larger the number of spins under consideration, the more realistic the model, because the real cluster is formed on the basis of the impurity in the infinite chain. For a large number of spins in the model, the correlated component of the spins lying far from the Ni spin should be strongly reduced due to the dimerization. Therefore the magnetic properties of the model cluster should be independent of the number of spins. The possible values of the total spin of the cluster arising due to the substitution of one Cu ion per Ni ion are $S = 1$ and $S = 1/2$. In order to obtain $S = 1$, the spin of the Ni ion must be uncompensated and therefore the Cu ions are divided into dimers in another way when compared to the undisturbed chain. The correlation of the dimerization in the neighbouring chains will be violated in this case. For the case of the total spin $S = 1/2$, the spin of the Cu–Ni pair is uncompensated. This total spin value does not cause the rearrangement of the dimer lattice except for when the single pair Cu–Cu is replaced by a Cu–Ni pair. Therefore the total spin $S = 1/2$ of the cluster corresponds to the lower energy of the perturbation of the dimerized lattice, and the $S = 1/2$ models with the finite number of spins are probably more realistic than the models with $S = 1$.

We have analysed the five- and six-spin models for the cluster. The five-spin model has $S = 1$ in the ground state and the six-spin model has $S = 1/2$. The three-spin cluster would be the simplest case, but it has $S = 0$ in the ground state and is therefore nonmagnetic. The four-spin model could not include dimers from both sides of the Ni ion.

The five- and six-spin clusters are shown schematically in figure 11 and are described

by the Hamiltonian

$$\mathcal{H} = \sum_{i,j}^{K}{}' J_{i,j}\boldsymbol{S_i}\cdot\boldsymbol{S_j} + \sum_{i,j}^{K}{}' \boldsymbol{D}_{i,j}\cdot\boldsymbol{S_i}\times\boldsymbol{S_j} + \sum_{i=1,\alpha=a,b,c}^{i=K} g_{i\alpha}\mu_B H_\alpha S_{i\alpha}. \qquad (5)$$

Here the $g_{i\alpha}$ are the g-tensor components for the Cu and Ni ions, and μ_B is the Bohr magneton. The J_{ij} are the nearest-neighbour and the next-nearest-neighbour exchange integrals and the $\boldsymbol{D}_{ij}$ are the vectors of the antisymmetric exchange. The different pairs of ions are taken into account only once in the sums $\sum'$. K is the number of spins, equal to 5 or 6.

In the following analysis we shall assume the $\boldsymbol{D}_{ij}$-vectors to be parallel to each other and perpendicular to the c-axes of the crystal. For the five-spin cluster the ions are labelled Cu_5–Cu_4–Ni_1–Cu_2–Cu_3 and the nonzero J_{ij} are taken as follows. $J_{54} = J_{23} = 10.6$ meV are the Cu–Cu exchange integrals; $J_{12} = J_{14} = 5$ meV are the exchange integrals for Ni and Cu ions—they are estimated as half of the Cu–Cu exchange integrals [33]; $J_{42} = 3.6$ meV is the next-nearest-neighbour exchange for the pure material [9]; J_{13} and J_{15}, the next-nearest-neighbour exchange integrals for the Ni ion, are taken to be 2 meV. The $\boldsymbol{D}_{ij}$-vectors are assumed to be parallel to each other and perpendicular to the chains.

The diagonalization of the Hamiltonian (5) gives the energy levels for $S = 1$ states of the five-spin cluster depending on the D_{ij}-values and magnetic field. The levels characterized with $S_z = 0, \pm 1$ are spilt by the D_{ij}-terms of (5). The transitions with the momentum change of $\pm\hbar$ are therefore separated by a gap of 1.0 meV in zero field. The formulae determining the gap and the values of the g-factor are given in the appendix. This gap is the main feature differentiating the $S = 1$ and $S = 1/2$ cases of the five- and six-spin models.

The lowest $S = 1/2$ states of the of the six-ion clusters are also separated by a gap which depends on the exchange integrals and D_{ij}-values. A magnetic field splits these levels; this splitting depends on the magnetic field and D_{ij}. However, the transitions between the sublevels with the $\pm\hbar$ momentum change remain gapless. The modification of the ESR spectrum at low frequencies is restricted here to the renormalization of the effective g-factors. The energy levels are obtained by the diagonalization of the 10×10 energy matrix for the $S = 1/2$ states of the six-spin cluster. For the cluster with the ions labelled Cu_5–Cu_6–Ni_1–Cu_2–Cu_3–Cu_4 with the following values of the exchange integrals: $J_{12} = 5$ meV, $J_{16} = 5$ meV, $J_{23} = 9.8$ meV, $J_{34} = J_{56} = 10.6$ meV, the terms dominating in the g-factors for the cases with the magnetic field perpendicular and parallel to the Dzyaloshinsky–Moriya vectors are

$$g_\perp \approx \frac{4g_{\mathrm{Ni}} - g_{\mathrm{Cu}}}{3} - \frac{4g_{\mathrm{Ni}} + 5g_{\mathrm{Cu}}}{9}\frac{(4D_{16} + 3D_{65})^2}{54E_{21}^2} \qquad (6)$$

$$g_\parallel \approx \frac{4g_{\mathrm{Ni}} - g_{\mathrm{Cu}}}{3} \qquad (7)$$

where

$$E_{21} \approx J_{56} - \frac{2}{3}J_{61} + \frac{1}{6}J_{62} - \frac{5}{9}J_{15} \qquad (8)$$

is the energy interval between the ground state and the lower excited state of the cluster.

To obtain $g_\perp = 1.6$ as observed in our experiments, we have to assume that $D_{16} \approx D_{65} \approx 3$ meV. The exact diagonalization of the matrix gives the close value of $|D_{ij}| = 3.4$ meV.

The values of the averaged spin projection at the site for the six-spin cluster obtained by the procedure described are given in table 2 and are shown schematically in figure 11. The

Table 2. The average values of the spin projections of the ions used in constructing a model six-spin cluster.

D_{ij}	S_5	S_6	S_1	S_2	S_3	S_4
0	0.16	−0.118	0.614	−0.145	0.007	−0.017
See the text	0.117	−0.125	0.591	−0.152	0.013	−0.02

following numerical values are used in this procedure in addition to the exchange integrals given above: $D_{12} = D_{16} = D_{23} = D_{34} = D_{65} = 3.4$ meV.

Thus the results obtained on the basis of the six-spin model correspond to the observed gapless ESR spectrum with the anisotropic g-factor deviating from the free-spin g-factor. The five-spin model does not correspond to the observed ESR signals due to the absence of a gap in the observed spectrum. Therefore the spectra obtained confirm the proposed $S = 1/2$ structure of the cluster.

Note that in our experiments we observed the reduction of the g-factor with decreasing temperature for all principal orientations of the magnetic field; while the model with collinear vectors $\boldsymbol{D}_{ij}$ predicts the deviation for only one principal direction, the g-factors for the other two principal directions should be close to 2. Nevertheless, these simple models demonstrate the possible mechanism for the reduction of the value of the effective g-factor and of its strong anisotropy. The deviation from the free-spin g-factor value of the other components of the g-factor tensor may probably be provided by any noncollinearity of the vectors $\boldsymbol{D}_{ij}$.

The nonlinearity of the magnetization curves at low temperatures which is shown in figure 10 also confirms the formation of spin clusters with their intrinsic degrees of freedom, because the energy levels of the cluster are separated by gaps depending in a nonlinear way on the magnetic field. The existence of a nonlinear susceptibility was reported as evidence for Dzyaloshinsky–Moriya interactions in three-ion clusters in [34]. The growth with temperature of the linear part of the susceptibility, visible in figure 10, is obviously due to the temperature dependence of the concentration of the triplet excitations of the spin–Peierls state. The nonlinear contribution to the magnetization curves diminishes and vanishes with the temperature rise from 1.6 to 6 K. At a temperature of about 9 K the magnetization curve again becomes nonlinear, but with the convexity directed down. The differential susceptibility grows with the magnetic field. This behaviour may be explained by the destruction of the spin–Peierls state by the applied magnetic field [35]. This destructive magnetic field could be of moderate magnitude when the temperature is close to T_{SP}.

The nonlinear magnetization curve at 2 K might be described as a sum of the linear $M(H)$ curve and of the magnetization of a paramagnet with the concentration of 10^{-3} $S = 1/2$ ions per Cu ion, the nonlinearity being ascribed to the paramagnetic saturation. However, the analogous curve for 6 K could not be described in this way because the characteristic field of the saturation is not shifted to higher fields.

The change of the g-factor of the Ni-doped samples with temperature may be ascribed to the freezing out of the reservoir of the triplet excitations of the spin–Peierls state below T_{SP}. It results in the switching off of the exchange narrowing and in the destruction of the collective character of the precession mode of the impurities and triplet excitations of the spin–Peierls state. This process is similar to the temperature evolution of the resonance spectrum of the triplet excitations in ion radical salts with a singlet ground state [36, 37]. At low temperatures only the impurity mode (the spin-cluster mode) survives, which leads to the unusual value of the g-factor. At intermediate temperatures the intermediate g-factor is observable, due to the exchange mixing of the spin states.

5. Conclusion

The data obtained correspond to an x–T phase diagram showing a linear dependence of T_{SP} and T_N on the doping concentration. From the AFMR spectra we found that the impurity-induced antiferromagnetism in $Cu_{0.968}Ni_{0.032}GeO_3$ can be described in terms of a molecular-field theory as a conventional orthorhombic antiferromagnet with the easy axis directed along $\boldsymbol{a}$, the hard axis along $\boldsymbol{b}$ and the second easy axis along $\boldsymbol{c}$. From AFMR spectra we obtained gaps of 22 and 33 GHz and anisotropy fields of $H_{a1} \sim 0.017$ T, $H_{a2} \sim 0.036$ T. The antiferromagnetic ordering of the 1.7% Ni-doped sample could not be considered within the molecular-field approximation because of the small value of the sublattice magnetization accompanied by the magnetically disordered spin–Peierls background. This results in the absence of a conventional AFMR spectrum. The anomalous value and temperature dependence of the g-factor in the spin–Peierls state of Ni-doped crystals indicates the formation of spin clusters around the doping magnetic ions. The presence of magnetic clusters with their own internal degrees of freedom is confirmed by observation of nonlinear magnetization curves in the magnetically disordered state. Further theoretical and experimental investigations of the cluster structure are necessary for a more detailed interpretation of ESR spectra and magnetization curves.

Acknowledgments

The authors are indebted to L A Prozorova, S S Sosin, I A Zaliznyak, M A Teplov and M V Eremin for valuable discussions.

This work was performed with the support of the Russian Foundation for Fundamental Research (grant number 98-02-16572) and the Civilian Research and Development Foundation, award N RP1-207. The work at the University of Warwick was supported by the EPSRC grant *Correlated Magnetic Systems* GR/K54021.

Appendix

The calculations of the energy levels of the five-ion linear cluster Cu_5–Cu_4–Ni_1–Cu_2–Cu_3 are based on the Hamiltonian (5). The energies of the three low-lying triplets with $S = 1$ are given approximately by

$$E_{1,2} = \frac{I_1 + I_{23}}{2} + \frac{I_2 + I_3}{4} \mp \frac{1}{2}\sqrt{\left(I_1 - I_{23} - \frac{I_2 + I_3}{2}\right)^2 + 2(I_{12} + I_{13})^2}. \tag{A1}$$

$$E_3 = \frac{1}{2}(I_3 + I_2) - I_{23}. \tag{A2}$$

where

$$I_1 = -\frac{3}{4}(J_{23} + J_{45}) \tag{A3}$$

$$I_2 = -\frac{1}{2}(J_{14} + J_{15}) - \frac{3}{4}J_{23} + \frac{1}{4}J_{45} \tag{A4}$$

$$I_3 = -\frac{1}{2}(J_{12} + J_{13}) - \frac{3}{4}J_{45} + \frac{1}{4}J_{23} \tag{A5}$$

$$I_{12} = \frac{1}{\sqrt{2}}(J_{14} - J_{15}) \qquad I_{13} = \frac{1}{\sqrt{2}}(J_{12} - J_{13}) \qquad I_{23} = \frac{1}{4}J_{24}. \tag{A6}$$

The Dzyaloshinsky–Moriya interaction splits the ground-state triplet into levels with the energies E_s, $E_{a,b}$:

$$E_s = E_1 \qquad E_{a,b} = E_1 - C_1^2 \frac{(\boldsymbol{G}_{12} - \boldsymbol{G}_{14})^2}{E_3 - E_1} \tag{A7}$$

where

$$\boldsymbol{G}_{12} = \frac{1}{4}(\boldsymbol{D}_{12} + \boldsymbol{D}_{23} - \boldsymbol{D}_{13}) \qquad \boldsymbol{G}_{14} = \frac{1}{4}(\boldsymbol{D}_{14} + \boldsymbol{D}_{45} - \boldsymbol{D}_{15}). \tag{A8}$$

$$C_1 = \frac{0.5(I_2 + I_3) + I_{23} - E_1}{\{[0.5(I_2 + I_3) + I_{23} - E_1]^2 + 0.5(I_{12} + I_{13})^2\}^{1/2}}. \tag{A9}$$

The energies in the magnetic field are determined by the secular equation

$$\begin{vmatrix} E_s - \varepsilon & g^x_{eff}\beta H_x & g^z_{eff}\beta H_z \\ g^x_{eff}\beta H_x & E_a - \varepsilon & \mathrm{i}g^y_{eff}\beta H_y \\ g^z_{eff}\beta H_z & -\mathrm{i}g^y_{eff}\beta H_{y,} & E_b - \varepsilon \end{vmatrix} = 0. \tag{A10}$$

Here g^x_{eff}, g^y_{eff} and g^z_{eff} are given by

$$g^x_{eff} = g^z_{eff} = \left[C_1^2 g_{\mathrm{Ni}} + \frac{1}{2}C_2^2(g_{\mathrm{Ni}} + g_{\mathrm{Cu}})\right]\left(1 - \frac{1}{2}\left(C_1\frac{\boldsymbol{G}_{12} - \boldsymbol{G}_{14}}{E_3 - E_1}\right)^2\right) \tag{A11}$$

$$g^y_{eff} = C_1^2 g_{\mathrm{Ni}} + \frac{1}{2}C_2^2(g_{\mathrm{Ni}} + g_{\mathrm{Cu}}) - \left(C_1\frac{\boldsymbol{G}_{12} - \boldsymbol{G}_{14}}{E_3 - E_1}\right)^2\left(C_1^2 g_{\mathrm{Ni}} + (0.5 - C_1^2)(g_{\mathrm{Ni}} + g_{\mathrm{Cu}})\right) \tag{A12}$$

where

$$C_2 = \frac{-(I_{12} + I_{13})/\sqrt{2}}{\{[0.5(I_2 + I_3) + I_{23} - E_1]^2 + 0.5(I_{12} + I_{13})^2\}^{1/2}}. \tag{A13}$$

The Dzyaloshinsky–Moriya vector $\boldsymbol{G}_{12} - \boldsymbol{G}_{14}$ is supposed to be parallel to the y-axis. When the external magnetic field is perpendicular to the vector $\boldsymbol{G}_{12} - \boldsymbol{G}_{14}$ and $E_s - E_a \gg g\beta H$ the frequency–field dependence is quadratic.

References

[1] Hase M, Terasaki I and Uchinokura K 1993 *Phys. Rev. Lett.* **70** 3651
[2] Pytte E 1974 *Phys. Rev.* B **10** 4637
[3] Nishi M, Fujita O and Akimitsu J 1994 *Phys. Rev. Lett.* **50** 6508
[4] Regnault L P, Ain M, Hennion B, Dhalenne G and Revcolevschi A 1996 *Phys. Rev.* B **53** 5579
[5] Hirota K, Cox D E, Lorenzo J E, Shirane G, Tranquada J M, Hase M, Uchinokura K, Kojima H, Shibuya Y and Tanaka I 1994 *Phys. Rev. Lett.* **73** 736
[6] Oseroff S, Cheong S-W, Fondado A, Aktas B and Fisk Z 1994 *J. Appl. Phys.* **75** 6819
[7] Honda M, Shibata T, Kindo K, Sygai S, Takeuchi T and Hori H 1996 *J. Phys. Soc. Japan* **65** 691
[8] Smirnov A I, Glazkov V N, Vasil'ev A N, Leonyuk L I, Coad S M, Paul D M^{c}K, Dhalenne G and Revcolevschi A 1996 *JETP Lett.* **64** 305
[9] Riera J and Dobry A 1995 *Phys. Rev.* B **51** 16 098
[10] Braden M, Wilkendorf G, Lorenzana J, Ain M, McIntyre G J, Behruzi M, Heger G, Dhalenne G and Revcolevschi A 1996 *Phys. Rev.* B **54** 1105
[11] Khomskii D, Geertsma W and Mostovoy M 1996 *Proc. 21st Int. Conf. on Low Temperature Physics (Prague, 1996); Czech. J. Phys. Suppl.* S6 **46** 3239
[12] Hennessy M J, McElwee C D and Richards P M 1973 *Phys. Rev.* B **7** 930
[13] Regnault L P, Renard J P, Dhalenne G and Revcolevschi A 1995 *Europhys. Lett.* **32** 579
[14] Lussier J-G, Coad S M, McMorrow D F and Paul D M^{c}K 1995 *J. Phys.: Condens. Matter* **7** L325
[15] Fukuyama H, Tanimoto T and Saito M 1996 *J. Phys. Soc. Japan* **65** 1182

[16] Weiden M, Richter W, Geibel C, Steglich F, Lemmens P, Eisener B, Brinkman M and Güntherodt G 1996 *Physica* B **225** 177
[17] Hase M, Uchinokura K, Birgeneau R, Hirota K and Shirane G 1996 *J. Phys. Soc. Japan* **65** 1392
[18] Hase M, Sasago Y, Uchinokura K, Kido G and Hamamoto T 1995 *J. Magn. Magn. Mater.* **140–144** 1691
[19] Hase M, Hagiwara M and Katsumata K 1996 *Phys. Rev.* B **54** R3722
[20] Coad S, Petrenko O, Paul D M^{c}K, Lussier J-G and McMorrow D F 1997 *Physica* B **239** 350
[21] Koide N, Sasago Y, Masuda T and Uchinokura K 1996 *Proc. 21st Int. Conf. on Low Temperature Physics (Prague, 1996); Czech. J. Phys. Suppl.* S4 **46** 1981
[22] Anderson P E, Liu J Z and Shelton R N 1997 *Phys. Rev.* B **56** 11 014
[23] Sasago Y, Koide N, Uchinokura K, Martin M C, Hase M, Hirota K and Shirane G 1996 *Phys. Rev.* B **54** R6835
[24] Nojiri H, Hamamoto T, Wang Z J, Mitsudo S, Motokawa M, Kimura S, Ohta H, Ogiwara A, Fujita O and Akimitsu J 1997 *J. Phys.: Condens. Matter* **9** 1331
[25] Smirnov A I, Glazkov V N, Leonyuk L I, Vetkin A G and Eremina R M 1998 *Sov. Phys.–JETP* at press
[26] Coad S, Lussier J-G, McMorrow D F and Paul D M^{c}K 1996 *J. Phys.: Condens. Matter* **8** 6251
[27] Nagamiya T, Yosida K and Kubo R 1955 *Adv. Phys.* **4** 1
[28] Abragam A and Bleaney B 1970 *Electron Paramagnetic Resonance of Transition Ions* (Oxford: Clarendon) ch 9
[29] Belinskii M I, Tsukerblat B S and Ablov A V 1974 *Fiz. Tverd. Tela* **16** 989
[30] Yablokov Yu V 1978 *J. Mol. Struct.* **46** 285
[31] Yablokov Yu V, Voronkova V K and Mosina L V 1988 *Paramagnetic Resonance of Exchange Magnetic Clusters* (Moscow: Nauka) (in Russian)
[32] Yamada I, Nishi M and Akimitsu J 1996 *J. Phys.: Condens. Matter* **8** 2625
[33] Eremin M V and Rakitin Yu V 1977 *Phys. Status Solidi* **80** 579
[34] Tsukerblat B S, Novotvortsev V M, Kuyavskaya B Ya, Belinskii M I, Ablov A V, Bazhan A N and Kalinnikov V T 1974 *Pis. Zh. Eksp. Teor. Fiz.* **19** 525
[35] Hase M, Terasaki I, Uchinokura K, Tokunaga M, Miura N and Obara H 1993 *Phys. Rev.* B **48** 9616
[36] Chesnut D B and Phillips W D 1961 *J. Chem. Phys.* **35** 1002
[37] McConnell H M, Griffith H O and Pooley D 1962 *J. Chem. Phys.* **36** 2518